Three-dimensional multispecies MHD studies of the solar wind interaction with Mars in the presence of crustal fields

Yingjuan Ma, Andrew F. Nagy, Kenneth C. Hansen, Darren L. DeZeeuw, and Tamas I. Gombosi

Space Physics Research Laboratory, Department of Atmospheric, Oceanic, and Space Sciences, University of Michigan, Ann Arbor, Michigan, USA

K. G. Powell

Aerospace Engineering Department, University of Michigan, Ann Arbor, Michigan, USA

Received 30 January 2002; revised 5 April 2002; accepted 13 May 2002; published 9 October 2002.

[1] We present the results of model calculations using a multispecies MHD model of the interaction of the solar wind with Mars. The three ions considered are H^+, O_2^+, and O^+, representing the solar wind and the two major ionospheric ion species, respectively. The calculations indicate that the presence of a hot oxygen corona does not, within the resolution and accuracy of the model, lead to any significant effect on the dayside bow shock and ionopause positions. Next the trans-terminator fluxes and escape fluxes down the tail were calculated neglecting the effects of the crustal magnetic field. The calculated flux values are consistent with the measured escape fluxes and the calculated limiting fluxes from the dayside ionosphere. Finally, a 60-order harmonic expansion model of the measured magnetic field was incorporated into the model. The crustal magnetic field did not cause major distortions in the bow shock but certainly had an important effect within the magnetosheath and on the apparent altitude of the ionopause. The model results also indicated the presence of ''minimagnetocylinders,'' consistent with the MGS observations. We also recalculated the trans-terminator and escape fluxes, for the nominal solar wind case, in the presence of the crustal magnetic field and found, as expected, that there is a decrease in the calculated escape flux; however, it is still reasonably close to the value estimated from the Phobos-2 observations. *INDEX TERMS:* 2780 Magnetospheric Physics: Solar wind interactions with unmagnetized bodies; 2459 Ionosphere: Planetary ionospheres (5435, 5729, 6026, 6027, 6028); 5440 Planetology: Solid Surface Planets: Magnetic fields and magnetism; 2728 Magnetospheric Physics: Magnetosheath; *KEYWORDS:* Mars, MHD, bow shock, escape flux, solar wind interaction, crustal magnetic field

Citation: Ma, Y., A. F. Nagy, K. C. Hansen, D. L. DeZeeuw, T. I. Gombosi, and K. G. Powell, Three-dimensional multispecies MHD studies of the solar wind interaction with Mars in the presence of crustal fields, *J. Geophys. Res.*, *107*(A10), 1282, doi:10.1029/2002JA009293, 2002.

1. Introduction

[2] The magnetometer carried aboard the Mars Global Surveyor (MGS) has clearly demonstrated that, like Venus, Mars does not have a significant, global, intrinsic magnetic field [*Acuna et al.*, 1998]. However, these measurements also established the presence of significant, local, small-scale, crustal, remnant magnetization [*Acuna et al.*, 1998]. Therefore, the global scale solar wind interaction with Mars is with the ionosphere-atmosphere system, but the presence of this remnant magnetization can have an important impact on some aspects of the interaction processes. Studies of the solar wind interaction with unmagnetized bodies (e.g., Venus, Mars, Titan) have been carried out in the past using semikinetic [e.g., *Brecht*, 1997], single and multispecies MHD [e.g., *Murawski and Steinolfson*, 1996; *Tanaka and Murawski*, 1997; *Tanaka*, 1998; *Bauske et al.*, 1998; *Shinagawa and Bougher*, 1999; *Liu et al.*, 1999, 2001] and two-ion [*Sauer et al.*, 1994, 1996] MHD model calculations.

[3] The single-fluid MHD calculations have, in general, considered the planet/moon as a perfectly conducting sphere. The so-called multispecies models used separate continuity equations for the solar wind and ionospheric ions (atomic and molecular oxygen ions), but they assumed that all ions have the same velocity and temperature. This formulation allowed the use of a much more realistic ionospheric inner boundary condition, but the single velocity assumption is a potential weakness. The two-ion model has the advantage of allowing for different ion velocities, but is only two-dimensional and assumes that the ion pressures are zero. Semikinetic calculations of the solar wind interaction with Venus and Mars have also used conducting spheres as inner boundary conditions. These latter model calculations

0148-0227/02/2002JA009293

have been especially useful in showing the lack of symmetry in the interaction processes. It has been argued that the use of semikinetic models is especially appropriate for Mars, where the ion gyroradius is of the same order as the planetary radius. However, it is important to note that the ideal MHD equations have been found to be successful even in such situations. The possible reason for this maybe the fact that, as shown by the semikinetic code, and observed by the Phobos-2 wave instrument [*Grard et al.*, 1989], and the MGS magnetometer [e.g., *Acuna et al.*, 1998; *Cloutier et al.*, 1999], significant wave activity and turbulence is present, leading to a wide variety of wave particle interactions, which in turn act as pseudocollisions.

2. Model and Numerical Method

[4] In this paper we present new results from our three-species ideal MHD calculations of the solar wind interaction with Mars. We solved the following set of normalized equations:

$$\frac{\partial \mathbf{W}}{\partial t} + \{\nabla \cdot \mathbf{F}\}^T = \mathbf{Q} \tag{1}$$

where the total energy density is defined as

$$\varepsilon = \frac{1}{2}\{\rho_1 + \rho_2 + \rho_3\}u^2 + \frac{1}{\gamma - 1}p + \frac{B^2}{2} \tag{2}$$

the state vector, flux tensor, and source vector in equation (1) are

$$\mathbf{W} = \begin{pmatrix} \rho_1 \\ \rho_2 \\ \rho_3 \\ \{\rho_1 + \rho_2 + \rho_3\}\mathbf{u} \\ \mathbf{B} \\ \varepsilon \end{pmatrix} \tag{3}$$

$$\mathbf{F} = \begin{pmatrix} \rho_1\mathbf{u} \\ \rho_2\mathbf{u} \\ \rho_3\mathbf{u} \\ \{\rho_1 + \rho_2 + \rho_3\}\mathbf{uu} + \left\{p + \frac{B^2}{2}\right\}\mathbf{I} - \mathbf{BB} \\ \mathbf{uB} - \mathbf{Bu} \\ \mathbf{u}\left\{\varepsilon + p + \frac{1}{2}\mathbf{B}\cdot\mathbf{B}\right\} - \{\mathbf{B}\cdot\mathbf{u}\}\mathbf{B} \end{pmatrix} \tag{4}$$

$$\mathbf{Q} = \begin{pmatrix} 0 \\ S_2 - L_2 \\ S_3 - L_3 \\ \{\rho_1 + \rho_2 + \rho_3\}\mathbf{g} - \{\rho_1 + \rho_2 + \rho_3\}\nu\mathbf{u} - \mathbf{u}L_2 - \mathbf{u}L_3 \\ 0 \\ Q_6 \end{pmatrix} \tag{5}$$

where the source term of the energy equation, Q_6, is

$$Q_6 = \{\rho_1 + \rho_2 + \rho_3\}\mathbf{u}\cdot\mathbf{g} - \frac{1}{2}u^2\{L_2 + L_3\} - \{\rho_1 + \rho_2 + \rho_3\}\nu u^2 - \frac{1}{\gamma - 1}\frac{L_2 p}{\{32\rho_1 + \rho_2 + 2\rho_3\}} - \frac{1}{\gamma - 1}\frac{L_3 p}{\{16\rho_1 + 0.5\rho_2 + \rho_3\}} + \frac{1}{\gamma - 1}S_2\frac{k}{m_2}T_o + \frac{1}{\gamma - 1}S_3\frac{k}{m_3}T_o \tag{6}$$

and where ρ_1, ρ_2 and ρ_3 are the H^+, O_2^+ and O^+ mass densities, respectively, S_2, S_3 and L_2, L_3 are the O_2^+, and O^+ mass source and loss rates, respectively, p is the total thermal pressure of the plasma, **u** is the velocity of the plasma, ν is the ion neutral collision frequency (taken to be 4×10^{-10} {[O] + [CO2]} s^{-1}, T_o is the temperature of the newly produced ions, γ is the ratio of specific heats (and taken to be 5/3) and the other symbols have their usual definition.

[5] The Viking 1 and 2 retarding potential analyzer (RPA) measurements [*Hanson et al.*, 1977] and subsequent theoretical models [*Chen et al.*, 1978; *Fox*, 1993] have shown that O_2^+ is the major dayside ion below about 300 km in the ionosphere of Mars and O^+ becoming important above about 200 km. Thus we selected H^+, O_2^+ and O^+ as the three ions to use in our three-species model. The chemical reactions that we considered for the production and loss of O_2^+ and O^+ ions are

$$CO_2 + h\nu \rightarrow CO_2^+ + e \tag{7}$$

$$O + h\nu \rightarrow O^+ + e \tag{8}$$

$$CO_2^+ + O \rightarrow O_2^+ + CO \tag{9}$$

$$CO_2^+ + O \rightarrow O^+ + CO_2 \tag{10}$$

$$O^+ + CO_2 \rightarrow O_2^+ + CO \tag{11}$$

$$O_2^+ + e \rightarrow O + O \tag{12}$$

We took the photoionization rate of CO_2 and O to be 7.3×10^{-7} and 2.73×10^{-7} s^{-1}, respectively [*Schunk and Nagy*, 2000]; these ionization rates are multiplied by cos(SZA) on the dayside, where SZA is the solar zenith angle and no ionization is assumed to be present on the nightside. The rates for the reaction shown in equations (9), (10), (11), and (12) were taken to be 1.64×10^{-10}, 9.6×10^{-11}, 1.1×10^{-9}, and 7.38×10^{-8} cm^3 s^{-1}, respectively [*Schunk and Nagy*, 2000]. We also made the reasonable assumption that $e \approx [O_2^+] + [O^+]$, which simplified the source term. The thermal component of the neutral atmosphere was assumed to consist of CO_2 and O; their density distribution was taken to be: $[CO_2] = 1 \times 10^{10} \exp\{-(z)-140/15.8\}$ and $[O] = 3 \times 10^8 \exp\{-(z-140)/43.5\}$ where the altitudes, z, are in km.

[6] In this paper we present the results of a number of different calculations. First we examined the potential role of the hot oxygen corona on our calculated bow shock and ionopause positions for the nominal solar wind case. Second we took our basic model and calculated the trans-terminator ion fluxes along with the fluxes escaping down the tail for nominal, high and low solar wind conditions (we did present the nominal results in an earlier paper [*Liu et al.*, 2001]). Finally, we studied the impact of the crustal magnetic fields [*Acuna et al.*, 1998] on the interaction processes, by using a harmonic expansion representation of the observed fields [*Arkani-Hamed*, 2001].

[7] A modified version of the BATS-R-US (Block Adaptive-Tree Solar wind Roe-type Upwind Scheme) has been developed to solve the three-species MHD equations described above. The BATS-R-US solution method is a

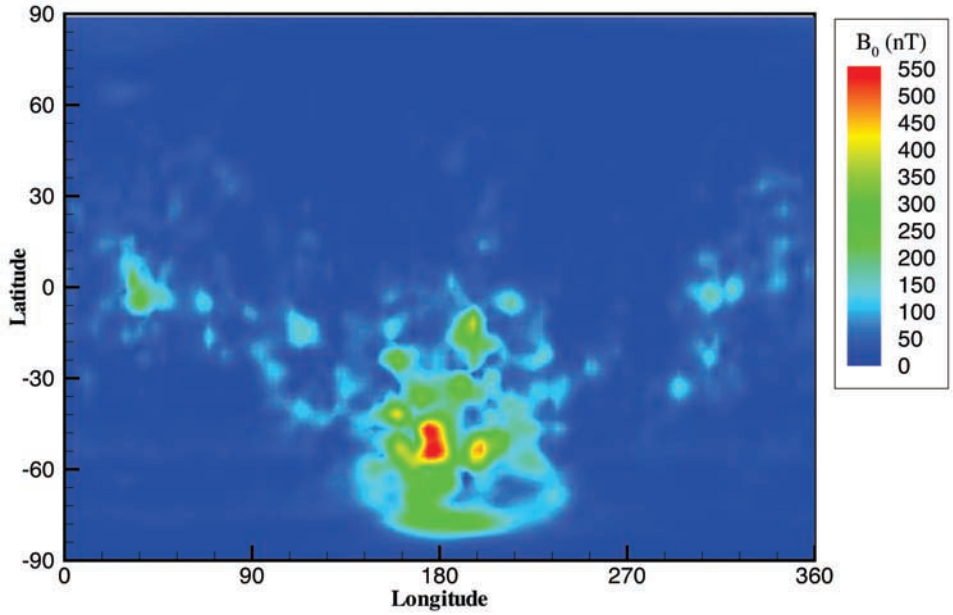

Figure 1. The remnant crustal magnetic field magnitude at an altitude of 200 km, calculated by using the 60-order harmonic expansion of *Arkani-Hamed* [2001].

highly scalable, massively parallel, block-adaptive mesh refinement (Block-AMR) algorithm developed for space physics applications that makes use of recent algorithmic advances in high-resolution upwind schemes. Details of the approach have been described elsewhere. Refer to the paper by *Powell et al.* [1999] for details.

[8] A computational domain defined by $-24\ R_M \leq x \leq 8\ R_M$, $-16 R_M \leq y, z \leq 16\ R_M$, where $R_M = 3396$ km is the radius of Mars, was used in the calculations and the inner boundary was taken to be 140 km above the Martian surface. An adapted grid consisting of 17,984 blocks and 1,150,976 computational cells was used in all of the simulations with the smallest cells having a dimension of about 53 km near the inner boundary and the largest cells, located in the nightside regions far from the planet, having a length of about 6792 km. The inner boundary conditions were specified as follows: $\rho_1 = 0.3\rho_{sw}$, where ρ_{sw} is the mass density of the undisturbed solar wind. This boundary condition is consistent with the expectation of very low H^+ densities in the lower ionosphere, similar to the situation at Venus [e.g., *Taylor et al.*, 1980]. The O_2^+ and O^+ densities at the inner boundary were taken to be the photochemical equilibrium value. A reflective boundary was used for **u**; this boundary condition for **u**, results in near zero velocities at the inner boundary and ionospheric velocities of a few km s^{-1} in the ionosphere, as expected, assuming Venus-like conditions [cf. *Miller and Whitten*, 1991]. The sum of the electron and ion temperatures at the inner boundary was assumed to be 3000°K and the pressure was set accordingly. The upstream solar wind ion and electron temperatures were set to be 5×10^4 and 3×10^5 °K respectively. The IMF was assumed to be a Parker spiral in the X-Y plane with an angle of 56 degrees and a magnitude of 3 nT and the solar wind velocity was selected to be 500 km s^{-1}, respectively. We picked the solar wind density to be 4 cm^{-3} for the nominal case and then chose double and half of this value for high and low solar wind pressure simulations, respectively.

[9] The magnetic field, **B**, was set to zero at the inner boundary for the runs associated with the first set of trans-terminator and tail flux calculations, as was the case for the study of the role of the hot oxygen corona. *Arkani-Hamed* [2001] developed a 60-degree harmonic expansion for the magnetic field, which matches the observations. We were provided with the expansion coefficients for a 60-degree expansion (J. Arkadi-Hamed, private communication, 2001). The resulting magnetic field is plotted in Figure 1, as a function of longitude and latitude, corresponding to an altitude of 200 km. The significant and localized fields in the southern hemisphere are clearly seen in this figure. We used this magnetic field model in our calculations aimed at assessing the role of the crustal magnetic field on the interaction processes.

3. Results

[10] The extensive computer resources necessary to run this model limit the number of cases that we are able to run.

Table 1. Calculated Trans-Terminator and Escape Fluxes, With No Crustal Magnetic Field Considered

	Nominal Case		High-Pressure Case		Low-Pressure Case	
	Terminator Flux (s^{-1})	Escape Flux (s^{-1})	Terminator Flux (s^{-1})	Escape Flux (s^{-1})	Terminator Flux (s^{-1})	Escape Flux (s^{-1})
O_2^+	4.35×10^{25}	2.61×10^{25}	4.57×10^{25}	3.41×10^{25}	4.25×10^{25}	1.92×10^{25}
O^+	0.53×10^{25}	0.45×10^{25}	0.58×10^{25}	0.51×10^{25}	0.57×10^{25}	0.42×10^{25}
Total	4.88×10^{25}	3.06×10^{25}	5.15×10^{25}	3.92×10^{25}	4.82×10^{25}	2.34×10^{25}

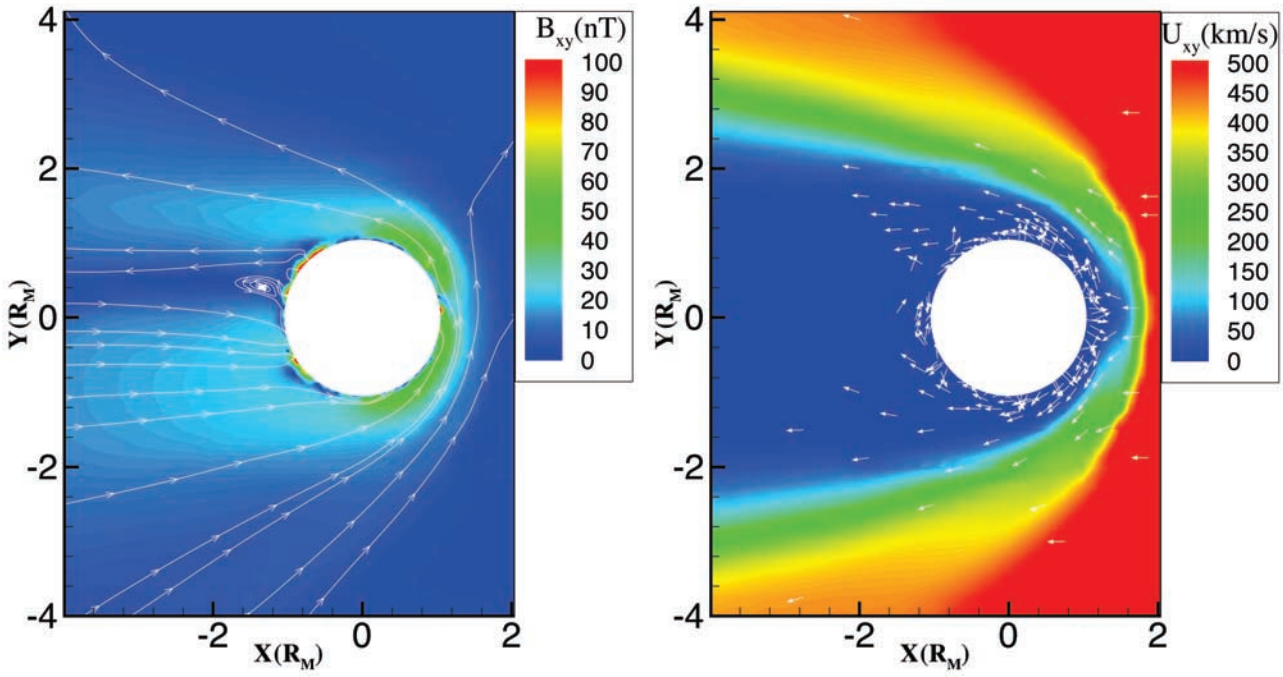

Figure 2. The component of the calculated magnetic field and velocity in the x-y plane. The color plots show the magnitudes; the white lines marked with arrows indicate the vector direction of the magnetic field and the arrows the direction (not the magnitude) of the velocity.

We used the NASA/GSFC and the NPACI, University of Texas Cray T3E parallel computers running on 256 processors; each run required about 1000 processor hours. We first carried out calculations for the nominal solar wind case for which we assumed no crustal magnetic field, but included a hot oxygen geocorona. The hot oxygen values were taken from the calculations of *Kim et al.* [1998], which are similar to the values obtained by *Hodges* [2000]. We

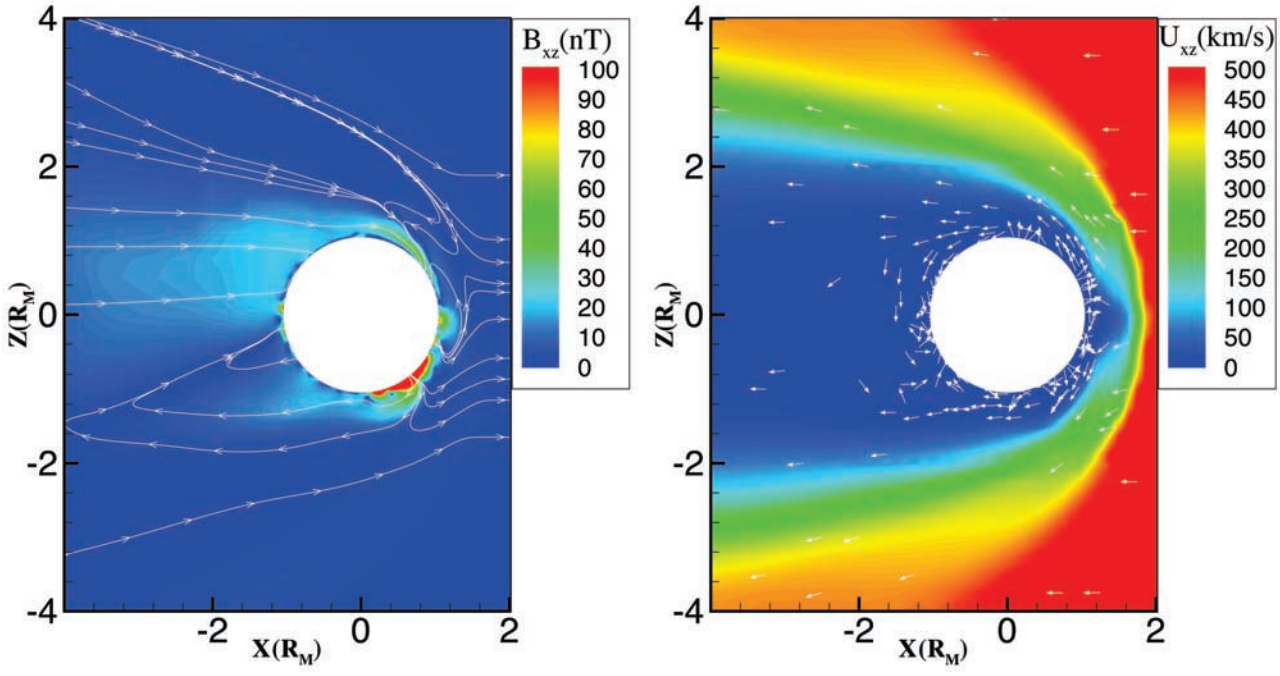

Figure 3. The component of the calculated magnetic field and velocity in the x-z plane. The color plots show the magnitudes; the white lines marked with arrows indicate the vector direction of the magnetic field and the arrows the direction (not the magnitude) of the velocity.

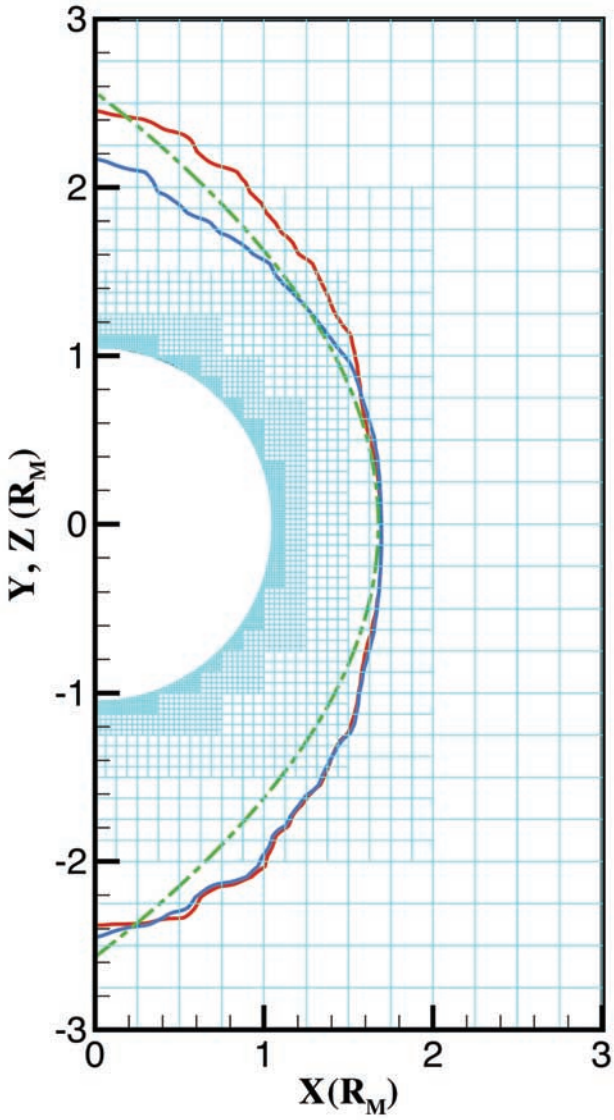

Figure 4. Plot showing where the magnetic field value is equal to 9 nT in the equatorial plane (blue line) and in the meridional plane (red line); this value of the magnetic field is used as a proxy for the location of the bow shock. Also shown is the mean value of the observed bow shock location (green line) from *Vignes et al.* [2000].

selected the solar maximum values, in order to maximize the possible impact of such a geocorona. We assumed that the hot oxygen densities are altitude dependent, but do not change with solar zenith angle on the dayside and that they are zero on the nightside. Given that we were specifically interested in maximizing the dayside results, this assumption is reasonable. We found that within the spatial resolution that our current model allows, no meaningful changes in the dayside bow shock or ionopause locations, compared to the case with no hot oxygen present in the model. The O^+ trans-terminator and escape flux do increase somewhat, but, as expected, not the O_2^+ ones. We did not include thermal or hot hydrogen in our calculations, but given the mass ratios and the relative densities [e.g., *Nagy and Cravens*, 1988], they are not believed to play an important role. In the model we consider photoionization only. It was shown by *Zhang et al.* [1993] that electron impact ionization may at times exceed photoionization by up to a factor of four, although *Krimsky and Breus* [1996] have criticized this conclusion. As we are trying to test for the "maximum" effect, in a further run we multiplied the subsolar solar cycle maximum photoionization rate of the hot oxygen by a factor of four and kept it a constant over the dayside. However, we still could not see any significant changes in the dayside bow shock or ionopause locations and only small differences in the O^+ fluxes.

[11] Next we calculated the cross-terminator plasma flow and the escape flux down the tail. Here again we assumed zero intrinsic magnetic field and nominal atmospheric densities and photoionization rates. We made these calculations for nominal, high and low solar wind pressure cases. The results are presented in Table 1. The O_2^+ fluxes are larger than the O^+ ones for all cases and, of course, the fluxes escaping down the tail are less than the trans-terminator values. This difference corresponds to the downward flowing plasma on the nightside, which helps to maintain the nightside ionosphere. *Fox* [1997] estimated the upper limit of the total dayside upward flux, which to all practical purposes must be equal to the nightward flow. She estimated this upper limit to be $(4.4–14.2) \times 10^{25}$ s^{-1}, which is consistent with our range of calculated trans-terminator flux values of $(4.82–5.15) \times 10^{25}$ s^{-1}. The range of our calculated escape flux, $(2.34–3.92) \times 10^{25}$ s^{-1} also compares favorably with the estimated value of a few times 10^{25} s^{-1}, based on the local flux measurements by the ASPERA instrument [*Lundin et al.*, 1989] and the TAUS instrument [*Rosenbauer et al.*, 1989] carried aboard Phobos-2

[12] Finally, we ran our numerical model to assess the effects of the crustal magnetic fields, using the nominal solar wind and atmospheric parameters. The calculations were carried out for the case where the location of the largest crustal field (180 longitude) was pointing sunward, and the solar wind flow direction was parallel with the equator of the planet. Figure 2 shows the calculated magnetic field and velocity components in the equatorial plane, while Figure 3 shows the same parameters in the noon-midnight meridional plane. The color plots show the magnitude of the magnetic field and velocity components; the white lines show the field line directions and the arrows indicate the direction (not the magnitude) of the velocities. The draping of the IMF is clearly visible in the equatorial plane as indicated in Figure 2; the small "bends and kinks" are the result of the crustal fields. There also appears to be a flux rope like feature; flux ropes have been observed by the MGS magnetometer [*Vignes et al.*, 2002]. The general trend of the plasma flow is upward and toward the terminator on the dayside and either downward into the ionosphere (helping to maintain the nightside ionosphere) or down the tail (and escaping from the planet) on the nightside. Figure 3 shows the presence of closed field lines (mini "magneto-cylinders"), the result of the "merging" of the crustal and IMF fields. The presence of such minimagnetospheres has been inferred by the electron reflectometer carried aboard the Mars Global Surveyor (MGS) spacecraft [*Mitchell et al.*, 2001]. In Figure 4 we plot the dayside location of the calculated 9 nT values (three times the assumed IMF field)

as the proxy for the bow shock position. In order to compare these results to the observed bow shock locations (which have been presented assuming symmetry about the *X* axis) we show the calculated curves in the X-Y and X-Z planes. The agreement between the calculations and observations are good, especially considering the fact that there is a scatter, of the order of one Mars radius, in the observed locations.

[13] Given the strong spatial variations in the crustal field the ionopause locations are not expected to be spherically symmetric around the planet. We plotted the location, in the X-Z plane, of the positions where the kinetic pressure of the ionospheric ions equals the sum of the magnetic pressure and the total (kinetic plus dynamic) solar wind proton pressure. The position of this pressure balance is a reasonable indicator of the ionopause location. Figure 5 shows these locations for both the nonmagnetic case as well as for the case with the crustal fields included. The figure shows that the presence of the crustal magnetic field does raise the "ionopause" altitude, consistent with observations [*Mitchell et al.*, 2002]. The largest outward movement is near the strongest field location and corresponds to an altitude increase of about 370 km (The grid structure used in the calculations is also indicated in this figure and is a guide to the resolution available). We also recalculated the trans-terminator and tailward escape fluxes for the nominal solar case, as shown in Table 2. We find that these fluxes decrease in the presence of the crustal field, as expected. However, note that even this decreased escape rate is consistent with the estimated value, of a few times 10^{25} s^{-1}, from the Phobos-2 measurements [*Lundin et al.*, 1989; *Rosenbauer et al.*, 1989].

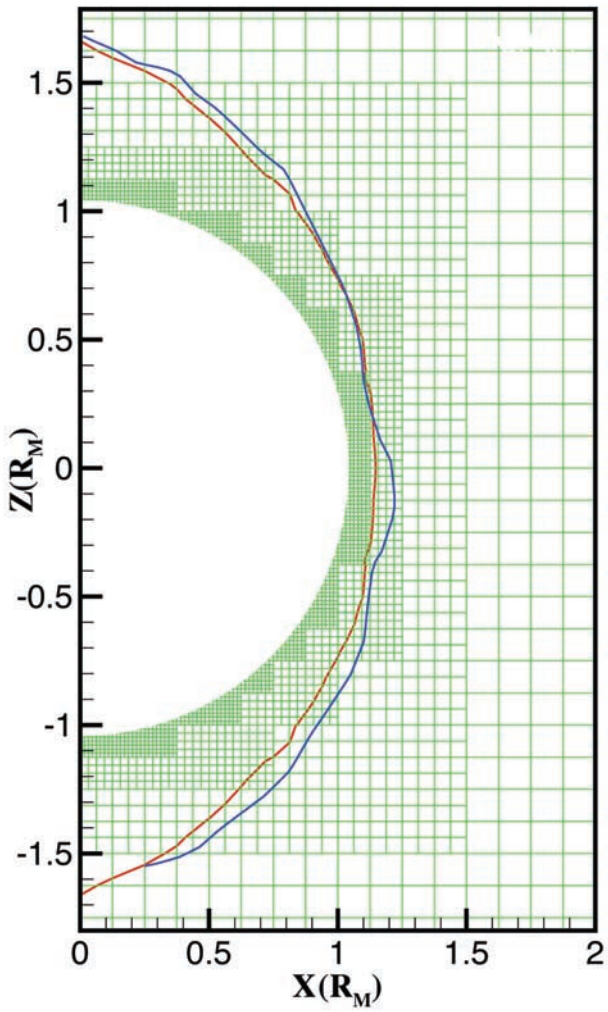

Figure 5. Plot showing the approximate location of the ionopause in the x-z plane for no crustal magnetic field (red line) and in the presence of such a field (blue line). The grid structure used in the calculations is also indicated.

Table 2. Calculated Trans-Terminator and Escape Fluxes for the Nominal Solar Wind Parameters and the Remnant Crustal Fields Considered

	Terminator Flux (s^{-1})	Escape Flux (s^{-1})
O_2^+	2.72×10^{25}	1.88×10^{25}
O^+	0.47×10^{25}	0.36×10^{25}
Total	3.19×10^{25}	2.24×10^{25}

4. Summary

[14] Here we presented the results of model calculations using our three species MHD model of the interaction of the solar wind with Mars. The three ions considered are H^+, O_2^+, and O^+, representing the solar wind and the two major ionospheric ion species, respectively. We showed results of calculations that indicated that the presence of a hot oxygen corona does not, within our resolution and accuracy, lead to any significant effect on the dayside bow shock and ionopause positions. Next we calculated the trans-terminator and escape fluxes down the tail, neglecting the effects of the crustal magnetic field. The calculated flux values are consistent with the measured fluxes and calculated limiting fluxes from the dayside ionosphere. Finally, we used a 60-order harmonic expansion model of the measured magnetic field and incorporated it into our model. The crustal magnetic field did not cause major distortions in the bow shock, but certainly had an important effect within the magnetosheath and some apparent effect on the altitude of the ionopause. Also our model results indicated the presence of "minimagnetocylinders", consistent with the MGS observations. We also recalculated the trans-terminator and escape fluxes, for the nominal solar wind case, in the presence of the crustal magnetic field. We found that, as expected, the presence of the crustal field caused the fluxes to decrease; however, the calculated escape flux was still close to the value estimated from the Phobos-2 observations. The next step in our model development is to change to spherical coordinates, which will allow much better altitude resolution, especially within the ionospheric region, and thus will help to elucidate the ionospheric interaction processes much better.

[15] **Acknowledgments.** We wish to thank J. Arkani-Hamed for providing us with his model of the remnant, crustal magnetic field prior to its publication. This work was supported by NASA grant NAG5-8946. We also gratefully acknowledge the computing resources made available for these studies at NASA/GSFC and the U. of Texas, NPACI facilities.

[16] Lou-Chuang Lee and Chin S. Lin thank Richard Hodges Jr. and Takeshi Tanaka for their assistance in evaluating this paper.

References

Acuna, M. H., et al., Magnetic field and plasma observations at Mars: Initial results of the Mars Global Surveyor Mission, *Science*, *279*, 1676, 1998.

Arkani-Hamed, J., A 50-degree spherical harmonic model of the magnetic field of Mars, *J. Geophys. Res.*, *106*, 23,197, 2001.

Bauske, R., et al., A three-dimensional MHD study of solar wind mass loading processes at Venus: Effects of photoionization, electron impact ionization, and charge exchange, *J. Geophys. Res.*, *103*, 23,625, 1998.

Brecht, S. H., Hybrid simulations of the magnetic topology of Mars, *J. Geophys. Res.*, *102*, 4743, 1997.

Chen, R. H., T. E. Cravens, and A. F. Nagy, The Martian ionosphere in light of the Viking observations, *J. Geophys. Res.*, *83*, 3871, 1978.

Cloutier, P. A., et al., Venus-like interaction of the solar wind with Mars, *Geophys. Res. Lett.*, *26*, 2685, 1999.

Fox, J. L., The production and escape of nitrogen atoms on Mars, *J. Geophys. Res.*, *98*, 3297, 1993.

Fox, J. L., Upper limits to the outflow of ion at Mars: Implications for atmospheric evolution, *Geophys. Res. Lett.*, *24*, 2901, 1997.

Grard, R., A. Pedersen, S. Klomov, S. Savin, A. Skalsky, J. G. Trotignon, and C. Kennel, First measurements of plasma waves near Mars, *Nature*, *341*, 607, 1989.

Hanson, W. B., S. Sanatini, and D. R. Zuccaro, The Martian ionosphere as observed by the Viking retarding potential analyzer, *J. Geophys. Res.*, *82*, 4351, 1977.

Hodges, R. R., Distributions of hot oxygen for Venus and Mars, *J. Geophys. Res.*, *105*, 6971, 2000.

Kim, J., A. F. Nagy, J. L. Fox, and T. E. Cravens, Solar cycle variability of hot oxygen atoms at Mars, *J. Geophys. Res.*, *103*, 29,339, 1998.

Krimsky, A. M., and T. K. Breus, Comment on "Oxygen ionization rates at Mars and Venus: Relative contributions of impact ionization and charge exchange", *J. Geophys.*, *101*, 1996.

Liu, Y., A. F. Nagy, C. P. T. Groth, D. L. DeZeeuw, T. I. Gombosi, and K. G. Powell, Three-dimensional multifluid MHD studies of the solar wind interaction with Mars, *Geophys. Res. Lett.*, *26*, 2689, 1999.

Liu, Y., A. F. Nagy, T. I. Gombosi, D. L. DeZeeuw, and K. G. Powell, The solar wind interaction with Mars: Results of three-dimensional three-species MHD studies, *Adv. Space Res.*, *27*, 1837, 2001.

Lundin, R., et al., First measurements of the ionospheric plasma escape from Mars, *Nature*, *341*, 609, 1989.

Miller, K. L., and R. C. Whitten, Ion dynamics in the Venus ionosphere, *Space Sci. Rev.*, *55*, 165, 1991.

Mitchell, D. L., R. P. Lin, C. Mazelle, H. Reme, P. A. Cloutier, J. E. P. Connerney, M. H. Acuna, and N. F. Ness, Probing Mars' crustal magnetic field and ionosphere with the MGS Electron Reflectometer, *J. Geophys. Res.*, *106*, 23,419, 2001.

Mitchell, D. L., R. P. Lin, H. Reme, P. A. Cloutier, J. E. P. Connerney, M. H. Acuna, and N. F. Ness, Probing Mars' crustal magnetic field and ionosphere with the MGS Electron Reflectometer, paper presented at XXXIII Lunar and Planetary Science Conference, contribution 2029, NASA, Houston, Tex., March 2002.

Murawski, K., and R. S. Steinolfson, Numerical simulations of mass loading in the solar wind interaction with Venus, *J. Geophys. Res.*, *101*, 2547, 1996.

Nagy, A. F., and T. E. Cravens, Hot oxygen atoms in the upper atmospheres of Venus and Mars, *Geophys. Res. Lett.*, *15*, 433, 1988.

Powell, K. G., P. L. Roe, T. J. Linde, T. I. Gombosi, and D. L. DeZeeuw, A solution-adaptive upwind scheme for ideal magnetohydrodynamics, *J. Comput. Phys.*, *154*, 284, 1999.

Rosenbauer, H., et al., Ions of Martian origin and plasma sheet in the Martian magnetosphere: Initial results of the TAUS experiment, *Nature*, *341*, 612, 1989.

Sauer, K., A. Bogdanov, and K. Baumgartel, Evidence of an ion composition boundary (protonopause) in bi-ion fluid simulations of solar wind mass loading, *Geophys. Res. Lett.*, *21*, 2255, 1994.

Sauer, K., E. Dubinin, K. Baumgartel, and A. Bogdanov, Bow shock "splitting" in bi-ion flows, *Geophys. Res. Lett.*, *23*, 3643, 1996.

Schunk, R. W., and A. F. Nagy, *Ionospheres: Physics, Plasma Physics, and Chemistry*, Cambridge Univ. Press, New York, 2000.

Shinagawa, H., and S. W. Bougher, A two-dimensional MHD model of the solar wind interaction with Mars, *Earth Planets Space*, *51*, 55, 1999.

Tanaka, T., Effects of decreasing ionospheric pressure on the solar wind interaction with non-magnetized planets, *Earth Planets Space*, *50*, 259, 1998.

Tanaka, T., and K. Murawski, Three-dimensional MHD simulation of the solar wind interaction with the ionosphere of Venus: Results of two-component reacting plasma simulation, *J. Geophys. Res.*, *102*, 19,805, 1997.

Taylor, H. A., et al., Global observations of the composition and dynamics of the ionosphere of Venus: Implications for the solar wind interaction, *J. Geophys. Res.*, *85*, 7765, 1980.

Vignes, D., et al., The solar wind interaction with Mars: Locations and shapes of the Bow Shock and Magnetic Pile-up Boundary from the observations of the MAG/ER experiment onboard Mars Global Surveyor, *Geophys. Res. Lett.*, *27*, 49, 2000.

Vignes, D., et al., Magnetic flux ropes in the Martian atmosphere: Global characteristics, in *The Interaction of the Solar Wind with Mars*, edited by D. Winterhalter, Kluwer Acad., Norwell, Mass., in press, 2002.

Zhang, M. H. G., J. G. Luhmann, A. F. Nagy, J. R. Spreiter, and S. S. Stahara, Oxygen ionization rates at Mars and Venus: Relative contributions of impact ionization and charge exchange, *J. Geophys. Res.*, *98*, 3311, 1993.

D. L. DeZeeuw, T. I. Gombosi, K. C. Hansen, Y. Ma, and A. F. Nagy, Space Physics Research Laboratory, Department of Atmospheric, Oceanic, and Space Sciences, University of Michigan, Ann Arbor, MI 48109, USA. (anagy@umich.edu)

K. G. Powell, Aerospace Engineering Department, University of Michigan, Ann Arbor, MI 48109, USA.